Parametric Study and Scaling of Axial-Flow-Induced Cylinder Vibration

Zongyan Lu and Yu Zhou

Abstract This work aims to conduct a parametric study on the flow induced vibration of an isolated elastic cylinder in axial flow. The cylinder with both ends fixed is free to vibrate in the lateral directions. Large eddy simulation and a two-way coupling CFD-CSM scheme are used to capture the turbulent flow and fluid–structure interaction, respectively. It has been found that the root-mean-square vibration amplitude $A_{rms}{}^{*}$ of the cylinder exhibits a considerable dependence on a number of parameters, including dimensionless flow velocity $\overline{U}$ (= 0.65–6.98), turbulence intensity T_u (= 0.7–6.0%), integral length scale $L_w{}^{*}$ (= 0.2–1.28) of the incident flow and cylinder length-to-diameter ratio L^{*} (= 20–43). It has been found from empirical scaling analysis that $A_{rms}{}^{*} = f_1(\overline{U}, T_u, L_w{}^{*}, L^{*})$ may be reduced to $A_{rms}/L = f_2(\overline{U}_{eff})$, where f_1 and f_2 are different functions and the scaling factor $\overline{U}_{eff}$ is interpreted as the effective Reynolds number. Several interesting inferences can be obtained from the scaling law.

Keywords Flow induced vibration · Parametric study · Scaling law

1 Introduction

The study of flow-induced vibration (FIV) on cylindrical structures subjected to axial flow is of both fundamental and practical importance because this vibration, albeit small in magnitude, may induce structural fretting, fatigue and even failure of nuclear reactors. In practice, axial incident flow is always turbulent. It has been experimentally found that structural response is sensitive to initial flow conditions [1–4]. For example, Modarres-Sadeghi et al. experimentally found the vibration amplitude of an elastic cylinder increases with increasing dimensionless flow velocity $\overline{U}$ $(= U_\infty L(\rho_f A_c/EI)^{1/2}$, where U_∞, ρ_f, L, A_c and EI are the free-stream velocity, fluid density, length and cross-sectional area of the cylinder and the corresponding

Z. Lu · Y. Zhou (✉)
Center for Turbulence Control, Harbin Institute of Technology, Shenzhen, China
e-mail: yuzhou@hit.edu.cn

D. Kim et al. (eds.), *Fluid-Structure-Sound Interactions and Control*, Lecture Notes in Mechanical Engineering, https://doi.org/10.1007/978-981-97-6211-8_18

flexural rigidity, respectively) [2]. In addition of $\overline{U}$, turbulence intensity T_u and integral length scale L_w^* are also two important parameters that characterize turbulent flow conditions. The asterisk denotes normalization by the cylinder diameter D in this paper. Note that $L_w = \frac{\bar{u}}{\overline{u'^2}} \int_0^{\tau_0} u(t)u(t+\tau)d\tau$, where τ_0 corresponds to the first zero crossing of auto-correlation function [5]. Wang et al. also experimentally observed that the vibration amplitude of the cylinder at high $T_u = 2.9\%$ is significantly increased compared with its counterpart at low $T_u = 0.7\%$ [3]. However, the information on how the characteristic flow parameters (e.g., L_w^* and T_u) affects flow-induced-vibration of the structures is very scarce in the literature. This motivates us to conduct a systematic parametric study on how the fluctuating vibration amplitude of an isolated elastic cylinder A_{rms}^* may vary with the characteristic parameters, including $\overline{U}$, T_u, L_w^* of incident flow as well as with cylinder length-to-diameter ratio L^*. Given $A_{rms}^* = f_1(\overline{U}, T_u, L_w^*, L^*)$, one may naturally beg the question: could we find a physically meaningful scaling factor ζ so that $A_{rms}^* = f_2(\zeta)$? There is no doubt that such a scaling law, if unveiled, can be of great significance to engineering applications.

2 Computational Detail

An elastic cylinder with a diameter $D = 25$ mm and length $L = 20D$ is immersed in a tubular axial flow (see Fig. 1). The two ends of the cylinder are fixed, i.e., the displacements of the grid nodes on these ends are zero. Note that the definition of coordinate system is shown in Fig. 1. The z-axis that aligned along the axis of the undeformed cylinder and the x-axis are defined as the lateral and the streamwise directions, respectively, with their origin at the center of the left surface of the cylinder (see Fig. 1). Apparently, $z = 0$ and $20D$ denote the upstream and downstream ends of the cylinder, respectively (Fig. 1). The cylinder is perfectly straight without any deformation initially (see Fig. 1) and may vibrate freely in the x–y plane under fluid forces. Axial incident flow is confined by a cylindrical wall, which is of the same length as the cylinder with a diameter of $12D$. The velocity-inlet and pressure-outlet boundary conditions are adopted as the flow boundary conditions on the inlet and outlet of flow domain, respectively.

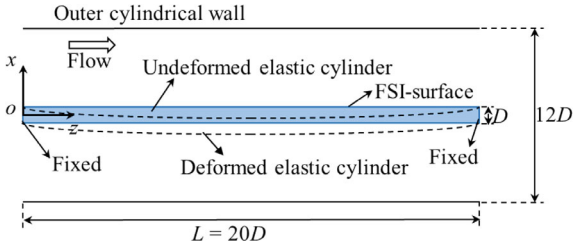

Fig. 1 Schematic of an elastic cylinder model

To simulate the interactions between the structure and its surrounding flow field, the dynamic equation of the cylinder and the governing equations of fluid flow are solved iteratively, which are given by

$$\mathbf{M}\ddot{\vec{d}} + \mathbf{K}\vec{d} = \vec{F}(t) \tag{1}$$

$$\nabla \cdot \vec{u} = 0 \tag{2}$$

$$\rho_f \frac{\partial \vec{u}}{\partial t} + \rho_f \left(\vec{u} - \hat{\vec{u}}\right) \cdot \nabla \vec{u} = -\nabla p + \mu \nabla^2 \vec{u} \tag{3}$$

where $\mathbf{M}$, $\mathbf{K}$, $\ddot{\vec{d}}$, $\vec{d}$ and $\vec{F}(t)$ are mass matrix, stiffness matrix, nodal acceleration vector, nodal displacement vector and load vector acting on the cylinder, respectively; $\vec{u}$, $\hat{\vec{u}}$ and p are the fluid velocity vector, moving mesh velocity vector and pressure, respectively.

The typical two-way coupling based on Ansys workbench is used to compute flow filed, Eqs. (2)–(3) and structural dynamics, Eq. (1), via iterations between the flow and structure solvers. The flow field imposes the forces on the cylinder to solve the cylinder displacement. The deformation of the cylinder updates its surrounding flow field, and subsequently, the flow field imposes new forces on the cylinder in the next iteration. The force and displacement are communicated on the fluid–structure interaction (FSI) surface (Fig. 1). The size of timestep Δt is 0.005 s. There are 8–12 coupling iterations per timestep. In order to capture the small-scale turbulent structures, the large eddy simulation (LES) is adopted along with Smagorinsky–Lilly subgrid scale model. The Smagorinsky constant C_s is 0.1. The second-order implicit method and a bounded central differencing scheme are adopted for time and space discretization, respectively. A comparison between experimental and numerical data and mesh independence have been made in our previous work [4].

3 Results and Discussions

Figure 2 illustrates that $A_{rms}{}^*$ varies with $\overline{U}$, T_u, $L_w{}^*$ and L^*. It is found that these four parameters produce a pronounced effect on $A_{rms}{}^*$. Clearly, $A_{rms}{}^*$ increases gradually with increasing $\overline{U}$ (Fig. 2a). In Fig. 2b, given $\overline{U} = 2.75$ and $L_w{}^* = 0.94$–1.08, the $A_{rms}{}^*$ grows from 0.017 to 0.035 with T_u increasing from 2.9 to 6.0%. The higher-intensity turbulence would penetrate into the shear layers around the elastic cylinder, interacting and destabilizing the shear layers around the cylinder. More small-scale eddies appeared in the vicinity of the elastic cylinder at high T_u [3]. These eddy-structures cause an increase in the flow fluctuations near the cylinder wall and lateral force on the cylinder, which account for the large $A_{rms}{}^*$. It is also observed from Fig. 2b that given same T_u, $A_{rms}{}^*$ increases with $L_w{}^*$. For instance, given $\overline{U} = 2.75$

and $T_u = 6.0\%$, $A_{rms}{}^*$ rises from 0.007 to 0.035 with $L_w{}^*$ increasing from 0.26 to 0.94. At a large $L_w{}^*$, the eddy-separation occurs from the cylinder-wall. The elastic cylinder absorbs energy from the excited flow field, causing the large $A_{rms}{}^*$. As a result, it is clear that given T_u, the $L_w{}^*$ has a non-negligible effect on flow field and thus on the vibration of the cylinder. It is surprisingly found that when $L_w{}^* = 0.6$ or 0.76, the $A_{rms}{}^*$ at $T_u = 6.0\%$ and $\overline{U} = 2.75$ is comparable to that at $T_u = 2.9\%$ and $\overline{U} = 6.55$ (Fig. 2b). Therefore, we might consider the high T_u effect on $A_{rms}{}^*$ as an additional $\overline{U}$, so as to establish a quantitative equivalent relationship between T_u and $\overline{U}$. As such, the scaling factor with the physical meaning may be obtained (as shown in Fig. 3).

An empirical scaling analysis has been performed to determine the intrinsic relationship between $A_{rms}{}^*$ and the four characteristic parameters. As demonstrated in Fig. 2a, for different L^* (= 43 and 20), the growth trend of relationship $A_{rms}{}^*$ with $\overline{U}$ resembles, i.e., nearly linear. Therefore, L^* might be considered for rescaling $A_{rms}{}^*$. It has been found that given T_u, the rescaled $A_{rms}{}^*/(L^*)$, i.e., A_{rms}/L, collapses well for different L^* (not shown). This implies that $A_{rms}{}^* = f_1(\overline{U}, T_u, L_w{}^*, L^*)$ could be

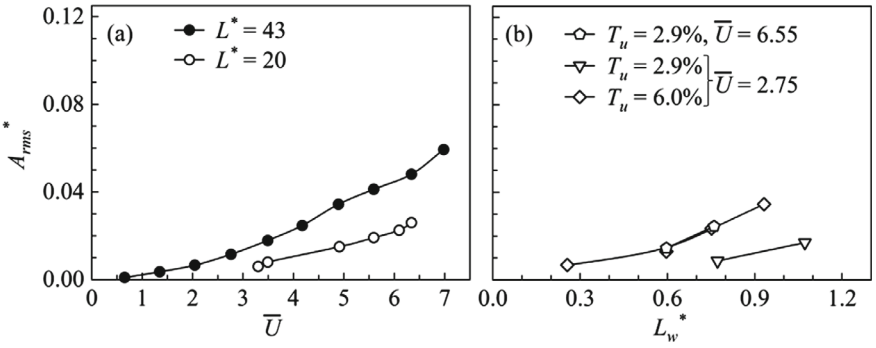

Fig. 2 Dependence of rms vibration amplitude of the cylinder $A_{rms}{}^*$ on **a** $\overline{U}$ and **b** $L_w{}^*$

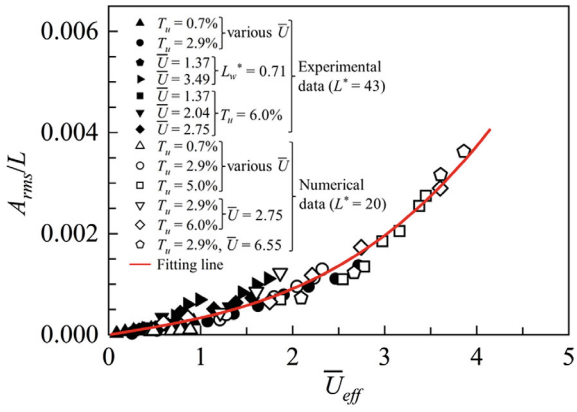

Fig. 3 Dependence of A_{rms}/L on scaling factor $\overline{U}_{eff}$

reduced to $A_{rms}/L = f_2(\overline{U}, T_u, L_w^*)$, where f_1 and f_2 are two different functions. Similarly, by replotting Fig. 2b, the dependence of A_{rms}/L on L_w/L at $\overline{U} = 2.75$ (not shown) further allows us to rescale A_{rms}/L via a new abscissa variable $T_u(L_w/L)$. As such, the function f_2 could be further reduced to $f_3(\overline{U}, T_u(L_w/L))$. It is known that cylinder amplitude exhibits a linear correlation with flow conditions and critical $\overline{U}$ for buckling, i.e., $\overline{U}_{crb}$ [6]. Subsequently, the function f_3 could be reduced to $f_4(T_u(L_w/L)\overline{U}/\overline{U}_{crb})$.

Figure 3 shows the scaling law of A_{rms}/L. It is surprisingly found that all the scattered data of A_{rms}/L collapse well once the scaling factor $\overline{U}_{eff} = EF \times \overline{U}/\overline{U}_{crb}$, instead of $T_u(L_w/L)\overline{U}/\overline{U}_{crb}$, is used as the abscissa, where EF is defined as $T_u(L_w/L)/[T_u(L_w/L)]_{\text{ref}}$. Subscript ref indicates the reference case where T_u is small, presently 0.7%, thus $EF \geq 1$. Now, the $\overline{U}_{eff}$ is physically interpreted as the effective Reynolds number that treats non-zero T_u or L_w^* effect on A_{rms}^* as an addition of $\overline{U}$. Note that $\overline{U}$ is directly proportional to Reynolds number in this paper. As shown in Fig. 3, all A_{rms}/L data are least-squares fitted to a curve, that is, the function f_4 is now reduced to $A_{rms}/L = f_5(\overline{U}_{eff})$. A departure of calculated/experimental data from the prediction of the curve is ascribed to differences in flow conditions between calculations and measurements. For instance, calculation is made under rather ideal conditions with a 'clean' environment but measurements are not, often associated with experimental uncertainties. Interesting inference can be made from the scaling law. Clearly, A_{rms}/L increases non-linearly with $\overline{U}_{eff}$, even though all $\overline{U}$, T_u, L_w^* changes. For instance, the A_{rms}/L substantially increases from 1.7×10^{-3} to 2.7×10^{-3} as $\overline{U}_{eff}$ increases from 2.75 to 3.45 (Fig. 3). Note that the two $\overline{U}_{eff} = 2.75$ and 3.45 corresponds to $(\overline{U}, T_u, L_w^*) = (2.75, 6.0, 0.92)$ and (6.10, 5.0, 0.64), respectively.

4 Conclusions

Numerical investigation has been carried out on the dependence on four parameters (i.e., $\overline{U}, T_u, L_w^*$ and L^*) of the flow-induced vibration amplitude A_{rms}^* of an isolated elastic cylinder in axial flow. This work leads to following conclusions.

1. The A_{rms}^* exhibits a strong dependence on $\overline{U}$, T_u, L_w^* and L^*. It has been found that, given the same T_u, A_{rms}^* may vary with L_w^* and vice versa, suggesting that both the turbulence level and its time or length scale of incident flow produce a pronounced effect on A_{rms}^*.
2. Empirical scaling analysis has been performed based on the experimental and numerical data. It has been found that $A_{rms}^* = f_1(\overline{U}, T_u, L_w^*, L^*)$ may be reduced to $A_{rms}/L = f_2(\overline{U}_{eff})$. The scaling factor $\overline{U}_{eff}$ is physically interpreted as the effective Reynolds number that treats non-zero T_u or L_w^* effect as an addition to the Reynolds number $\overline{U}$. Based on the scaling law, it is interestingly found that A_{rms}/L increases nonlinearly with $\overline{U}_{eff}$.

Acknowledgements Authors wish to acknowledge the financial support from China-Guangdong Nuclear Power Group through Grant No. CGN-HIT202221 and 91952204 from the National Natural Science Foundation of China, and from the Research Grants Council of the Shenzhen Government through Grant No. JCYJ20210324132816040.

References

1. Mulcahy TM, Yeh TT, Miskevks AJ (1980) Turbulence and rod vibrations in an annular region with upstream disturbances. J Sound Vib 69(1):59–69
2. Modarres-Sadeghi Y, Païdoussis MP, Semler C, Grinevich E (2008) Experiments on vertical slender flexible cylinders clamped at both ends and subjected to axial flow. Phil Trans R Soc A 366:1275–1296
3. Wang P, Wong CW, Zhou Y (2019) Turbulent intensity effect on axial-flow-induced cylinder vibration in the presence of a neighboring cylinder. J Fluids Struct 85:77–93
4. Lu ZY, Wong CW, Zhou Y (2020) Turbulence intensity effect on the axial-flow-induced vibration of an elastic cylinder. J Fluids Struct 99:103144
5. Giulio V, Hassan H, Thomas A, Charalampos B (2018) Generating atmospheric turbulence using passive grids in an expansion test section of a wind tunnel. J Wind Eng Ind Aerodyn 178:91–104
6. Chen YN (1970) Flow-induced vibration in tube bundle heat exchangers with cross and parallel flow, part I: parallel flow. In: Flow-induced vibration in heat exchangers, pp 57–66